ADVANCED MATERIALS
www.advmat.de

Band Structure Engineering at Heterojunction Interfaces via the Piezotronic Effect

*Jian Shi, Matthew B. Starr, and Xudong Wang**

Engineering the electronic band structure using the piezopotential is an important aspect of piezotronics, which describes the coupling between the piezoelectric property and semiconducting behavior and functionalities. The time-independent band structure change under short-circuit condition is believed to be due to the remnant piezopotential present at the interface, a result of the finite charge-screening depth at the interface. A series of materials, including metals, semiconductors and electrolytes, are selected to investigate the interfacial band structure engineered by remnant piezopotential when they are in contact with a strained piezoelectric semiconductor. The remnant piezopotential at the interface can switch the junction between Ohmic and Schottky characters, enhance charge combination/separation, regulate barrier height, and modulate reaction kinetics. The difference between the regular time-dependent, pulse-type piezopotential and constant remnant piezopotential is also discussed in detail using a ZnO-based photoelectrochemical anode as an example. The piezotronic effect offers a new pathway for engineering the interface band structure without altering the interface structure or chemical composition, which is promising for improving the performance of many electronics, optoelectronics, and photovoltaic devices.

1. Introduction

The piezotronic effect describes the coupling of piezoelectric polarization and the intrinsic electric field in a space charge region for the purpose of tuning charge transport behaviors of semiconductor materials and devices.[1–5] Semiconductors are technologically interesting because their electronic properties can be tailored from that of an insulator (10^{-9} Ohm·cm) to that of a good conductor (10^{3} Ohm·cm).[6] Critically, these properties can be modulated from one to the other by the presence of an adequate electric field.[7–9] Useful devices often require the integration of two or more materials that individually posses optimized properties (electron-hole mobility's, dielectric constants, indirect-direct band gaps, etc.) that are ideally suited for a specific purpose. The interface between these two dissimilar materials is called a heterojunction, which often possesses specific electronic properties that endow the device with the majority of its functionality.[10] Thus, while the electronic properties of the bulk semiconductors themselves are important, so are the properties of the interface at which these dissimilar materials (and their disparate band structures) make contact. Heterojunction have found use in many modern devices, including: transistors, singe and tandem solar cells, photoelectrochemical (PEC) cells, light emitting diodes (LEDs), quantum wells, photodetectors and semiconducting lasers to name but a few.[6,11,12]

The bases of modern technology (information processing, energy conversion and energy storage systems) all make use of how electrons flow through a circuit. In a heterojunction, the effect of an energy state discontinuity is profound, with the electronic conduction properties taking on a character that is exquisitely sensitive (exponentially dependent) to the magnitude of the discontinuity. It is via this means that the electronic properties of the ensemble can be dominated by the electron properties of the interface. It then follows axiomatically that the electronic properties of the ensemble can be tailored by precise modification of the interfacial energetics. To that end the piezoelectric potential could have a significant influence on the heterostructure's electronic properties (i.e., piezotronics), which requires either that a material composing the heterojunction must be piezoelectric or that a material within the near vicinity must be piezoelectric. It is thus advantageous that many of the materials used in the heterojunction devices listed previously are themselves piezoelectric, these include AlN, GaN, ZnO, CdS, SiC etc.[13] The precise application of mechanical deformation to the heterostructure results in a piezoelectric potential which can tailor the electronic properties of the interface. The merit of this approach is that it allows for a device to be composed of materials which are still individually optimized for their specific bulk electronic and optical properties while allowing the independent optimization of their heterointerface.

In 2007, Wang et al. first demonstrated that the piezoelectric potential produced by a deflected ZnO nanowire (NW) could regulate its longitudinal conductivity.[14] Following

J. Shi,[+] M. B. Starr,[+] Prof. X. D. Wang
Department of Materials Science and Engineering
University of Wisconsin-Madison
Madison, WI 53706, USA
E-mail: xudong@engr.wisc.edu
[+] These authors contributed equally to this work.

DOI: 10.1002/adma.201104386

 © 2012 WILEY-VCH Verlag GmbH & Co. KGaA, Weinheim

research further revealed a variety of semiconductor performance changes based upon the appearance of piezoelectric potential.[15–18] In this paper, we will discuss the relationships between piezoelectric potential and the band structure of a series of heterojunctions and how this effect influences the design and performance of heterojunction semiconductor devices.

2. Piezopotential in an Ideal Semiconductor

The direct piezoelectric effect describes a simultaneous shift in positive and negative charge centers within the primitive unit cell induced by a material deformation. The polar field which results from the direct piezoelectric effect will naturally interact with charged species present in the solid, i.e., nuclei and electrons, both localized and delocalized, in a Coulombic manner. In order to better understand the repercussions of this interaction, principally its effects on charge carrier conduction throughout the solid, it is instructive to invoke band theory. Band theory allows the facile representation of the electronic structure of matter by projecting *both* the energy of states which the electrons *do* occupy in the solid and *can* occupy in the solid as the ordinate and a real space dimension as the abscissa. **Figure 1**a depicts that band diagram for a semiconductor at 0 K in the absence of an internal electric field.

In the presence of a piezoelectric field, a voltage gradient will manifest itself in the band diagram as a slope with a magnitude equal to that of the voltage profile (Figure 1b). In the absence of mobile charged species and under an open-circuit condition, the piezoelectric potential remains fully unscreened and the magnitude of resultant voltage gradient is equal to that of the induced piezoelectric potential ϕ_{PZ}. At finite temperatures, free charge carriers will exist within the solid and their quantity will depend upon the temperature, band gap, and dopant concentration. These opposing free charges will segregate under the influence of the piezoelectric potential to opposite sides of the semiconducting material and in doing so establish an electric field which is counter to that of the piezoelectric field. This counter-piezo field will compensate to varying degrees the field remaining within the semiconducting material, acting most effectively to negate the field present in the center of the material.[19]

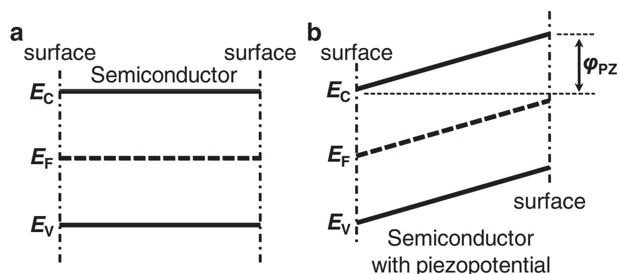

Figure 1. Schematic band structure diagrams of an ideal semiconductor (at T = 0 K) without (a) and with (b) the appearance of piezoelectric potential (E_c: conduction band; E_v: valence band).

Dr. Xudong Wang is an assistant professor in the department of Materials Science and Engineering at the University of Wisconsin–Madison. He received his PhD degree from Georgia Tech in 2005. His current research interests include understanding the coupling effect of semiconductor properties and piezoelectric polarization, and studying the growth and assembly of nanostructures for mechanical and solar energy harvesting.

Jian Shi obtained his B.S. degree in Materials Science and Engineering at Xi'an Jiaotong University in 2006, M.S. Degree in Mechanical Engineering at the University of Missouri-Columbia in 2008, and is currently finishing his Ph. D degree under the supervision of Prof. Xudong Wang in Materials Science Program at the University of Wisconsin-Madison. His research focuses on the nucleation and growth of oxide nanomaterials, photovoltaics, photoelectrochemical cells, nanogenerators and piezotronics.

Matthew Starr is a graduate student in Materials Science Program at the University of Wisconsin-Madison under the advisement of Prof. Xudong Wang. He received his B.Sc in Materials Science and Engineering at Rutgers University in 2009. He is interested in the electronic properties of materials. His current research focuses on fundamental understanding of the interaction between piezoelectricity and electrochemistry.

3. Remnant Polarization in Strained Piezoelectric Materials

The remnant polarization in ferroelectric materials is a well known phenomenon and has been intensively studied for decades.[20–24] Similarly, a strained piezoelectric material can also produce a permanent polarization that induces a

© 2012 WILEY-VCH Verlag GmbH & Co. KGaA, Weinheim

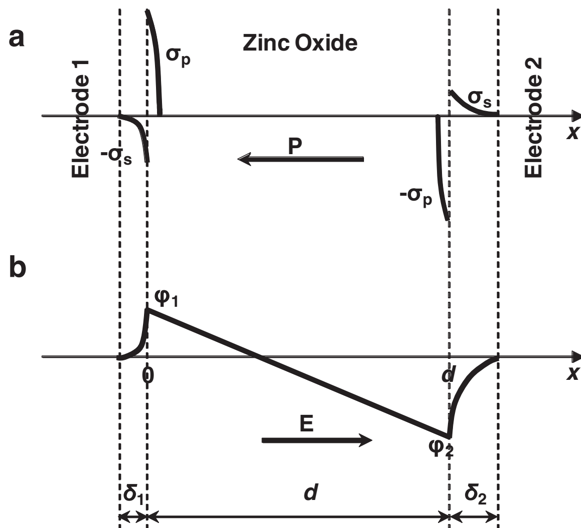

Figure 2. Schematic diagrams of the charge density distributions (a) and potential profiles (b) in ZnO and the two electrodes.

remnant piezopotential at the piezoelectric material-electrode interface under a short-circuit condition. This phenomenon can be understood via the same model used for ferroelectric materials.[20,25,26]

In a simplified one-dimensional model, a strained ZnO piezoelectric film is sandwiched between two electrodes (either metal or semiconductor) (**Figure 2**a). At steady state when the two electrodes are short circuited, the piezoelectric polarization P in the ZnO film creates surface charge densities $\pm\sigma_P$, which induce screening charge densities $\mp\sigma_S$ on the two electrodes in accordance with the following equation:

$$\sigma_S = \frac{d}{\varepsilon_r\,(\delta_1 + \delta_2) + d} \cdot P \tag{1}$$

where δ_1 and δ_2 are the charge screening lengths of the two electrodes, respectively, d the thickness of ZnO film, and ε_r the relative permittivity of ZnO. (Note that: for simplicity, P is regarded as the remaining piezoelectric polarization after internal free charge compensation. Therefore, under this condition, ZnO can be roughly equivalent to a ferroelectric material without free charge.) The remnant polarization is the result of incomplete external free charge compensation due to $\sigma_P > \sigma_S$ in a non-ideal electrode material ($\delta \neq 0$) and is given by:

$$\left|\varphi(0) - \varphi(d)\right| = \frac{d}{\varepsilon_r \varepsilon_0} \cdot (P - \sigma_S) \tag{2}$$

This potential difference is shared between the two electrode-ZnO interfaces and is determined by their charge screening lengths:

$$\left|\varphi_{1,2}\right| = \left|\varphi(0) - \varphi(d)\right| \frac{\delta_{1,2}}{\delta_1 + \delta_2} \tag{3}$$

The screening length can be determined to first order by the Thomas-Fermi screening length approximation for degenerated semiconductors[11] or the Debye screening radius for regular semiconductors.[27] Thus, the remnant piezopotential spatial distribution is schematically shown in Figure 2b. A linear potential drop is located within the ZnO and defined by the interface potential ϕ_1 and ϕ_2, which decays exponentially in the screening regions of the two electrodes. The potential profile at the interface changes the band structure accordingly. The amplitude of the band shift is therefore dependent on the magnitude of piezoelectric polarization as well as the materials used for surface contacts.

4. Interface Band Engineering by Remnant Piezopotential

The remnant piezopotential is a steady-state effect (as long as the strain is held) and thus will make a constant influence toward the band structure. We have shown that the remnant piezopotential can be determined by the electrode screening length. Therefore, different electrode materials can offer different interfacial band structure changes induced by remnant piezopotential. For example, in a semiconductor-piezoelectric material-metal (SC-P-M) system, the semiconductor electrode undertakes the majority portion of the remnant piezopotential due to its much longer screening length, which leads to a pronounced piezotronic effect at the SC-P interface. In this section, several representative heterojunction systems, including metal, semiconductor, and electrolyte contacts will be discussed in details to reveal the interfacial band structure engineered by remnant piezopotential, as shown in **Figure 3**.

Figure 3a shows the case of a metal-piezoelectric semiconductor (M-P) interface, where a Schottky contact is present. The original band structure is shown by dashed lines, and the band structure under remnant piezopotential is sketched in solid lines. Situations of positive and negative remnant piezopotential at the M-P interface are illustrated in the left and right diagrams, respectively. As discussed in the previous section, the peak remnant piezopotential appears at the M-P interface. The potential caused by screening charges in the metal side decays exponentially within a very narrow region (<0.1 nm).[25] Thus, change of the electronic band at the metal side can be negated. Superimposing the remnant piezopotential profile onto the original semiconductor band structures resolves the shifted band structure, as shown by the solid lines. The greatest band shifting exists at the interface while the band structure remains unchanged far from the interface. With a positive remnant piezopotential at the M-P interface, the barrier height is reduced. A sufficiently large remnant piezopotential (greater than the Schottky barrier height) can convert the Schottky barrier to Ohmic (left diagram in Figure 3a). When negative remnant piezopotential appears at the M-P interface, the barrier height becomes more pronounced and a Schottky diode with higher threshold voltage is obtained. The piezotronic concept utilized for Schottky barrier engineering provides a new mechanism for augmentation of electronic conduction actuated by mechanical strain.

Semiconductor-piezoelectric semiconductor (SC-P) heterojunction is another large category of solid state devices. In this system, the SC component can be regarded as one electrode having a much larger screening length than that of a metal (a few tens of nanometers). As discussed in the previous

© 2012 WILEY-VCH Verlag GmbH & Co. KGaA, Weinheim

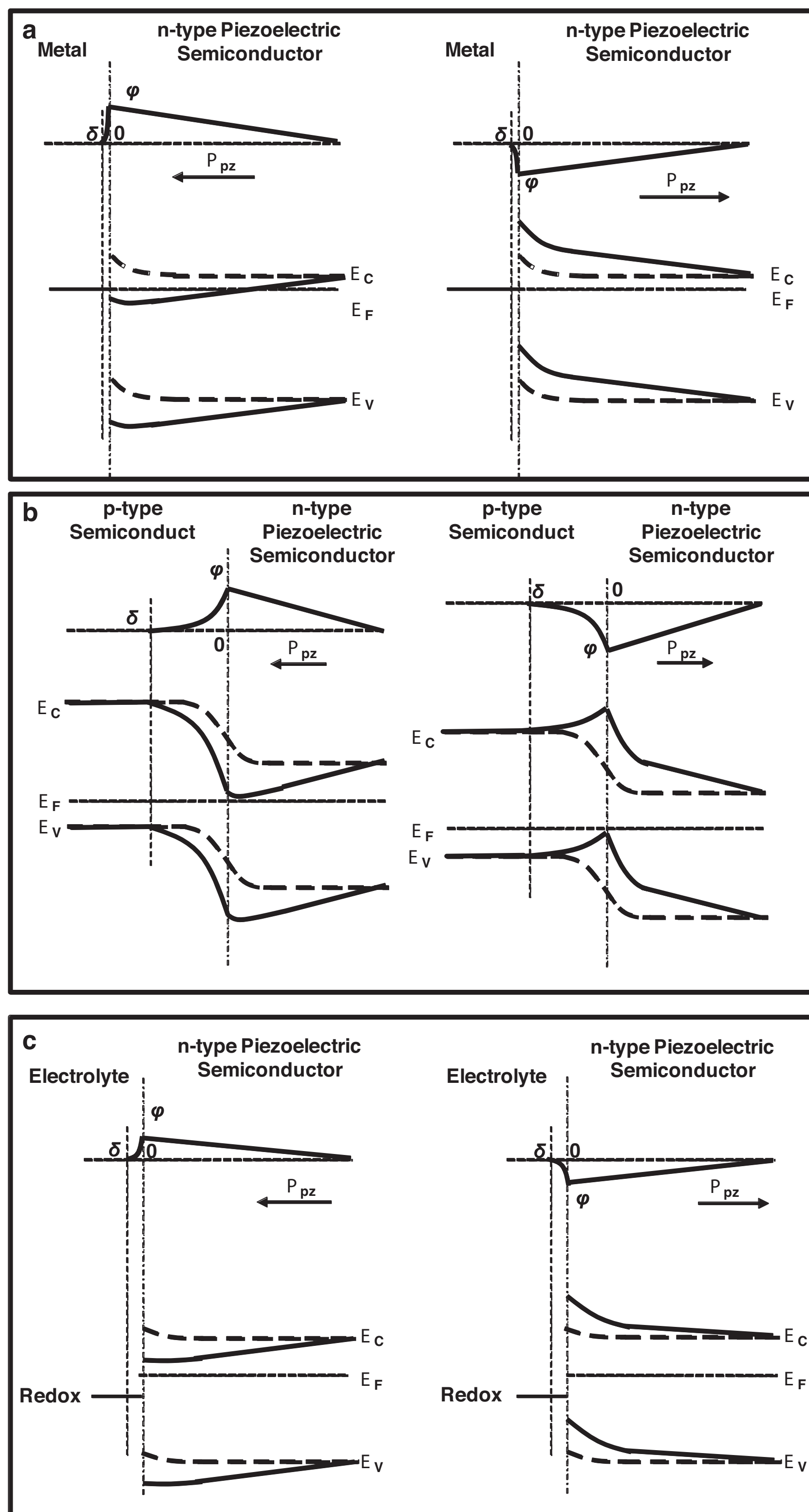

Figure 3. Schematic diagrams of the band structure change induced by remnant piezopotential when the electrodes are metal (a), semiconductor (b), and electrolyte (c), respectively. The cases of positive and negative remnant piezopotential at the interface are shown in the left- and right-hand-side diagrams, respectively.

section, electrodes possessing a long screening length will result in strong remnant polarizations and thus a pronounced remnant piezopotential, which induces remarkable band bending at the SC-P interface. Figure 3b illustrates the effect of remnant piezopotential on a p-n junction, where the original band structure is presented by the dashed lines. In the presence of remnant piezopotential at the interface, the piezoelectric material side shows the same tilting result as the M-P system. However, due to the broadness of potential profile on the p-type semiconductor's side, the band structure change is prominent and cannot be ignored. Such interface band bending (both positive and negative) influences the carrier states and can either improve or reduce the quantum efficiency of the heterojunction.

As a third case, the interface between electrolyte and piezoelectric semiconductor (El-P) is selected. Such interfaces are essential for many energy conversion and storage systems.[28] A main factor determining a semiconductor's ability to drive oxidation or reduction reactions at the semiconductor/electrolyte interfaces is the band bending present at the interface that either favors hole (upward bending) or electron transfer (downward bending). Therefore, through the application of remnant piezopotential to gain influence over interface energetics, and thus band bending, one can determine the redox reaction favored at the interface through strain, as shown in Figure 3c. In this case, electrolyte is regarded as one electrode which has a very high density of states and electrical conductivity, as is the case for most (practical) electrochemical systems operating under reasonable electrolyte concentrations.[27] This results in a very small screening length in the electrolyte, as is the case of metal electrodes. Therefore, only band bending on the piezoelectric semiconductor side is considered. For example, as shown in the left diagram of Figure 3c, original band bending at the El-P interface favors hole transfer from piezoelectric semiconductor to electrolyte for oxidation reactions. In the case of a sufficiently large remnant piezopotential present at this interface, the band bending can be reversed to favor electron transfer towards solution for reduction reactions. A negative remnant piezopotential (right diagram in Figure 3c) facilitates hole transfer and thus enhances the oxidation reaction.

Beyond the qualitative analysis, a number of experimental results have recently been shown to follow well with the interfacial band

© 2012 WILEY-VCH Verlag GmbH & Co. KGaA, Weinheim

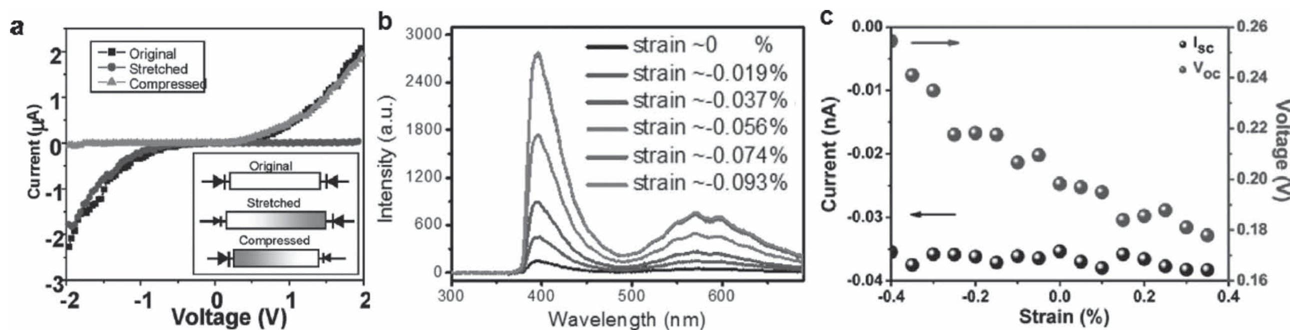

Figure 4. a) *I–V* characteristics of a Ag-ZnO-Ag system under zero, compressive and tensile strains. b) Electroluminescence spectra of a p-GaN/n-ZnO LED subject to different strains at a bias of 9 V. c) Strain dependent open circuit voltages and short circuit currents of a polymer (P3HT-ZnO) solar cell. Reproduced with permission.[29,30,32] Copyright.

engineering models. Using a ZnO nanowire (NW) as the piezoelectric semiconductor, Zhou et al. demonstrated a strain-induced *I–V* characteristic change in a Ag-ZnO-Ag system that consists of back-to-back Schottky barriers (**Figure 4**a).[29] This system can be represented by the M1-P-M2 model, where both electrodes are metals (approximately equal screening lengths) and thus both share the same magnitude but opposite sign of potential change at the interface. This produces the asymmetrical *I–V* curves, which makes the utilization of the M1-P-M2 structure as a memory switch possible. Yang et al. reported a dramatic improvement in the emission intensity of an n-ZnO/p-GaN based LED diode by straining the ZnO microwire component (Figure 4b).[30] This is the case of SC-P, where the remnant piezopotential forms a potential dip at the ZnO/GaN interface, which traps electron and/or holes and facilitates their recombination at the interface. Similar to LEDs, in the case of a GaN/InGaN quantum well laser, the quantum well profile can be rectified by a remnant piezopotential at the well's interface. Depending on the polarity of this potential, a negative or positive effect on the quantum efficiency can be obtained.[31] One extreme case of this model is the condition under which one side of the piezoelectric semiconductor is in contact with an insulator (M-P-I), for instance, a polymer. Depending on its electrical permittivity, the screening length of the polymer can be fairly large and the depolarization field within the piezoelectric material becomes prominent. The first demonstration of this configuration was realized in a polymer solar cell, in which ZnO microwires served as electron conductors and poly(3-hexylthiophene) (P3HT) was the photon absorber.[32] By straining the ZnO wires, while under photo illumination, the electric transport properties of the cells were modified resulting in a strain dependant open circuit voltage. Meanwhile, photocurrent remained essentially constant (Figure 4c).

The piezotronic concept also applies to ferroelectric materials, when their semiconductor functionality is of the major concern. For example, using the remnant ferroelectric polarization in place of strain-induced piezoelectric potential, spatially dependent photo deposition of Ag has been achieved on ferroelectric material, i.e., $BaTiO_3$ or PZT (lead zirconate titanate).[33–35] The photo deposition of Ag was observed on polarization domains orientated with the electric field vector pointing towards the semiconductor-electrolyte interface, while absence of Ag deposition was observed on domains exhibiting the opposite polarization.[36] **Figures 5**a and 5b show the polarization patterns on a PZT surface and Figures 5c and 5d illustrate that the deposition of Ag

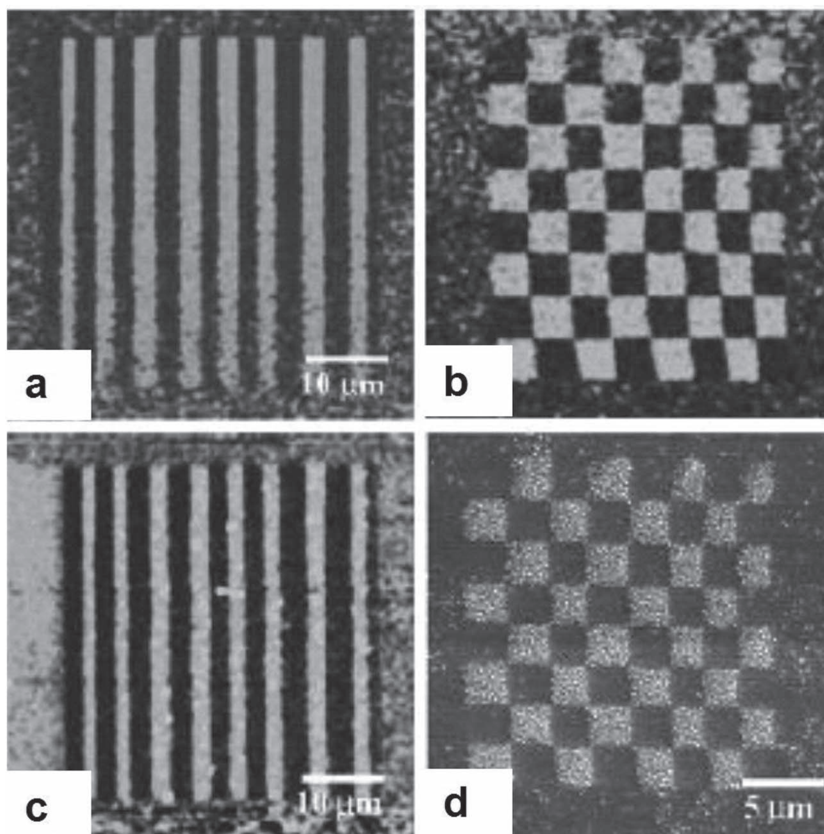

Figure 5. a,b) Piezoresponse force microscopy images of a PZT surface with alternating domain patterns that were poled by +10 V and –10 V DC voltage, respectively. c) Surface topography of sample (a) after photo deposition of Ag nanoparticles. d) Scanning electron microscopy image of sample (b) after photo deposition of Ag nanoparticles. Reproduced with permission.[36]

© 2012 WILEY-VCH Verlag GmbH & Co. KGaA, Weinheim

follows well with such patterns. However, these ferroelectric materials may not be ideal choices for electrochemical electrodes because of their low conductivity and high permittivity; whereas piezoelectric semiconductors, whose conductivities can be much higher, offer a balance between piezoelectric polarization and charge transport properties and could serve as good candidates in the design of piezo-enhanced electrode materials.

5. A Quantitative Study of Interface Barrier Height Engineering

We recently demonstrated th remnant piezopotential-induced interface barrier height change using a ZnO-based PEC anode fabricated by sputtering a thin film of ZnO (~1 µm thick) on an ITO/PET substrate.[37] The variation in interfacial band lineup between an ITO transparent electrode and a semiconductor electrode is a well-known issue. Based on the reported electron affinities and work functions of ITO and ZnO,[10] the equilibrium band lineups of the complete ZnO PZ-PEC water splitting system is schematically shown in **Figure 6**a. The larger work function of ZnO resulted in a small barrier, ϕ_{Bn} at the interface, which was evidenced by *I–V* characterization. Figures 6b and 6c present the photocurrent density (J_{ph}) measured by the potentiostat when a constant strain was applied to the ZnO anode periodically, where the applied external bias was fixed as 1.5 V versus SCE. With a compressive strain of –0.12%, J_{ph} decreased from 542 µA/cm^2 to 509 µA/cm^2 during an illumination intensity of 100 mW/cm^2. While with a tensile strain of 0.12%, J_{ph} increased from 269 µA/cm^2 to 287 µA/cm^2 under an illumination intensity of 50 mW/cm^2. The response of J_{ph} upon straining was swift and highly reproducible. More importantly, the J_{ph} change (ΔJ_{ph}) was independent of time. No decay was observed during a period extending over hundreds of seconds, as long as the strain was held (not including the initial spikes). ΔJ_{ph} is thus defined as the difference between the constant J_{ph} under strain and the J_{ph} base line when no strain was applied.

For a Schottky barrier-like heterojunction, the *J–V* characteristic is governed by:[6]

$$J = C_0 T^2 \exp\left[\frac{-q\left(\varphi_{Bn} + \Delta\varphi_{pz}\right)}{kT}\right]\left[\exp\left(\frac{qV}{nkT}\right) - 1\right] \quad (4)$$

where C_0 is a constant, q elementary charge, k Boltzmann constant, T temperature, n ideality factor, V applied potential, ϕ_{Bn} original barrier height, and $\Delta\phi_{pz}$ effective barrier height change by remnant piezopotential. This equation shows that even if the remnant piezopotential-induced barrier height change is small, the variation in current can still be significant. Using the $\Delta J_{ph}/J_{ph}$ data obtained from PEC measurements, $\Delta\phi_{pz}$ was calculated as a function of strain and represented by the squares in Figure 6d. The relation between $\Delta\phi_{pz}$ and strain appeared to be linear, with a barrier height decrease of ~1.5 mV per 0.1% strain applied. This relationship corresponds to a ~6% PEC efficiency enhancement per 0.1% strain.

The strain and barrier height change relationship can also be estimated using Equations (1)–(3). In the case where ITO and electrolyte are the two short-circuited electrodes in contact with a ZnO film, the interfacial barrier height change $\Delta\phi_{pz}$ is given by:

$$\Delta\varphi_{pz} = \varphi_1 = \frac{\delta_{ITO} d}{\varepsilon_0\left[\varepsilon_r\left(\delta_{ITO} + \delta_{electrolyte}\right) + d\right]} d_{31} E\varepsilon \quad (5)$$

where d_{31}, E and ε are the piezoelectric coefficient, Young's modulus and strain of the ZnO anode. Based on Thomas-Fermi screening length approximation, δ_{ITO} and $\delta_{electrolyte}$ were calculated to be 0.14 nm and 0.25 nm, respectively.[27,38] Calculation revealed a linear relationship between $\Delta\phi_{pz}$ and strain (solid curve in Figure 6d) with a slope (–1.14 mV/0.1%) slightly smaller than the experimental result (–1.5 mV/0.1%), which was likely due to deviation in the screening length estimation. This analysis further demonstrated that the remnant polarization and barrier height change is dependent on the materials used and their interfacial properties. A more pronounced barrier height change is expected at the interface of ZnO and other semiconductor materials that have longer screening length than ITO.

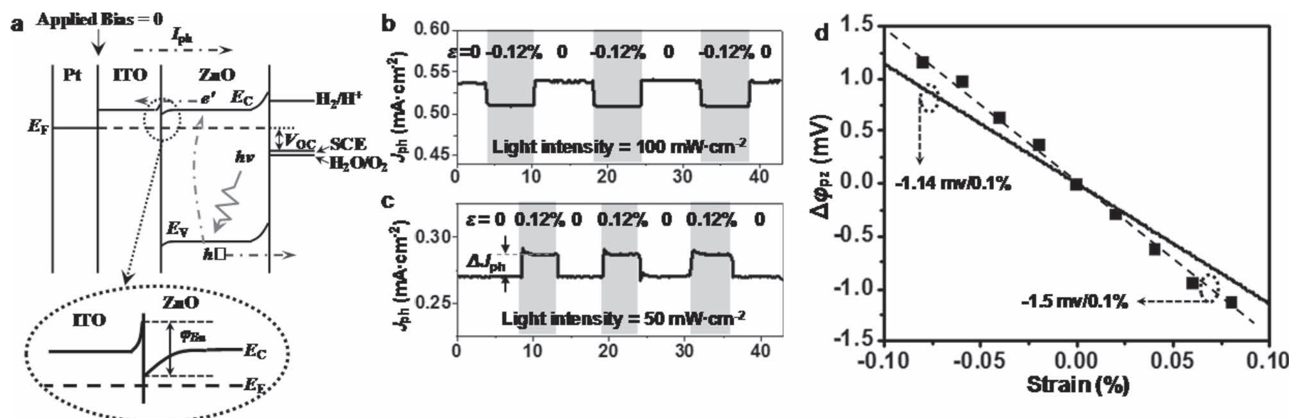

Figure 6. a) Schematic illustration of the band lineup of the ZnO PEC system. The detailed band alignment of the ITO/ZnO interface is shown in the dashed ellipse. b,c) Photocurrent density (J_{ph}) of the ZnO PZ-PEC under periodic compressive strains (–0.12%) b) and tensile strains (0.12%) c) at an applied bias of 1.5 V versus SCE. d) $\Delta\phi_{pz}$ determined from experimental results (squares) and by calculation (solid line).

© 2012 WILEY-VCH Verlag GmbH & Co. KGaA, Weinheim

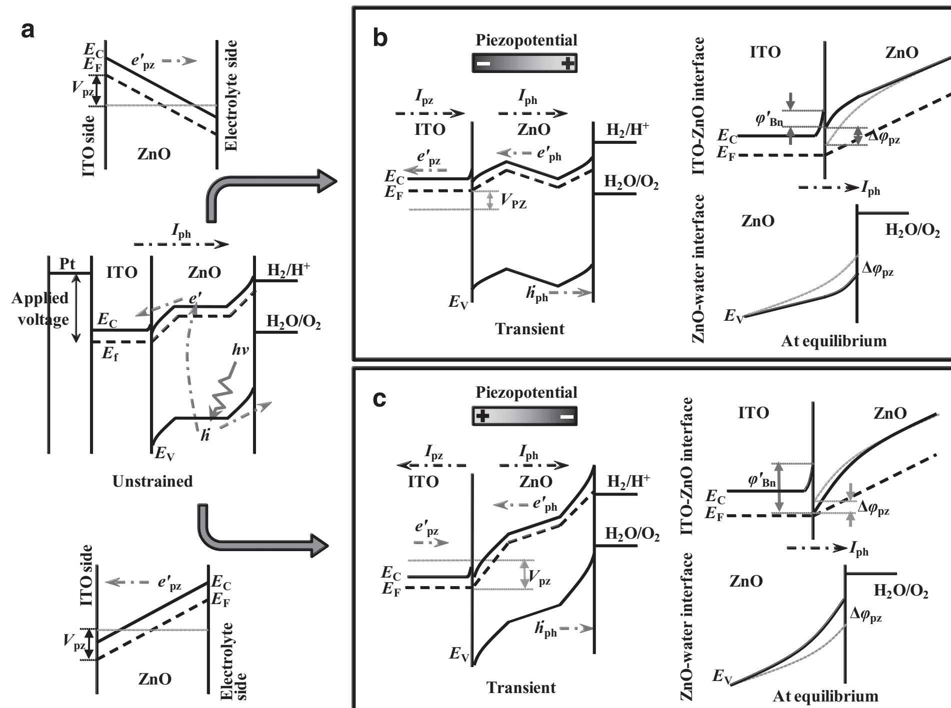

Figure 7. Band structure of the ZnO/ITO PEC anode for explaining the strain-induced photocurrent change. a) Middle diagram: Schematic band diagram of the ZnO/ITO PEC system when an external bias is applied between working electrode (ZnO/ITO) and counter electrode (Pt gauze). No strain is applied to the ZnO anode. Top and bottom graphs show the piezoelectric potential induced instantaneous band tilting in ZnO when the ZnO film is subject to tensile and compressive strain, respectively. b,c) Band alignment of the working ZnO/ITO anode during tensile (b) and compressive (c) strains. Left diagrams illustrate the transient band structure immediately after straining, where no charge screening is assumed to occur through the external circuit. The conduction and valence bands inside ZnO are the superposition of space charge-induced band shifting and instant polarization-induced band bending. Right diagrams are the steady-state band alignment after charge redistribution is completed, while ZnO is still under strain for the ITO/ZnO (top) and ZnO/electrolyte (bottom) interfaces. The remnant piezopotential at the heterogeneous interface shifts the bands from their original position (dashed curves) to a new position (solid lines), and thus changes the interface barrier height.

6. Distinguishing the Effects of Piezopotential and Remnant Piezopotential

The band structure change induced by remnant piezopotential is a static effect, which can lead to a constant current change. It is fundamentally different from the time-dependant current or voltage pulses produced by the direct piezoelectric effect. Electronic band theory is thus adopted to distinguish these two effects and fully understand the observed J_{ph} charecteristics when the ZnO PEC anode is under strain. Before the analysis, two basic aspects should be clarified. *First, the band structure of the PEC cell when a DC bias is applied between the Pt cathode and the PEC anode through the ITO* (center diagram of **Figure 7**a). Due to the non-zero free charge concentration in ZnO under illumination, a portion of the applied potential drops in the depletion region of ZnO at the ITO/ZnO and ZnO/electrolyte interfaces. *Second, the band structure of a ZnO thin film under strain* (top and bottom diagrams of Figure 7a for negative and positive piezopotential on ITO side, respectively). As discussed earlier, the piezoelectric potential induces a linear tilt of the bands and Fermi level along the thickness direction of the ZnO film. This band bending causes immediate free charge redistribution inside the ZnO film and results in a recovery of band flatness. Thus, the measured piezoelectric potential (V_{pz}) represents the amplitude of the surface Fermi level shifting after internal free charge screening.

Superimposing the piezopotential-induced band tilting with the original biased band structure reveals the transient band structure during the application of strain (left graph of Figures 7b and 7c for negative and positive piezopotential on ITO side, respectively). The transient stage is defined as the imaginary moment when the piezopotential-driven external charge transport has not yet occurred but the internal charge redistribution is completed. This situation is rationalized because of the small thickness of the ZnO film and the large impedance of the external circuit between the two ZnO surfaces. At this stage, the bulk conduction band and the Fermi level of ITO remain flat following the band edge of ZnO and the shifting amplitude is V_{pz}. This is the maximum voltage that can be measured. It should be noted that the initial ITO/ZnO interface band bending does not change at this moment because no charge redistribution has occurred across the interface. The V_{pz} will quickly drop to zero due to charge transport through the external circuit driven by the piezopotential as indicated by the arrow of e'_{pz}. Therefore the measured V_{pz}'s are always in the form of pulses. V_{pz} is directly proportional to the amplitude of strain and decreases with the increasing incident light intensity.

© 2012 WILEY-VCH Verlag GmbH & Co. KGaA, Weinheim

The piezoelectric-effect-related current change can now be understood using negative piezopotential as an example (tensile strain applied). As shown in the left diagram of Figure 7b, under illumination and an external bias, J_{ph} flows from ITO through ZnO to the electrolyte. The strain-induced V_{pz} creates an instantaneous piezocurrent (J_{pz}) with the same direction as J_{ph}. Therefore, a quick increasing of current density ($J_{ph} + J_{pz}$) is observed (as marked in Figures 8a–c). J_{pz} drops together with V_{pz}, resulting in a positive current pulse when a tensile strain is applied. When the Fermi level of ITO moves back to its original position due to J_{pz}, it is assumed the piezo-PEC system has reached a steady-state stage, although the anode is still under mechanical tension.

At the steady-state, the piezopotential is completely screened outside of the ITO space charge region and no more piezocurrent can be induced ($J_{pz} = 0$). However, due to the non-ideal interface of ITO/ZnO and ZnO/electrolyte (i.e., finite screening length), there always exists a remnant polarization at both interfaces. The remnant negative piezopotential at the ITO/ZnO interface locally moves up the conduction band of ZnO, as shown in the top-right diagram of Figure 7b, where the amplitude of the interface band shift is denoted as $\Delta\phi_{pz}$. A similar effect can also be induced in ITO. However, due to the very narrow depletion layer of ITO, band shifting on the ITO side is ignored here. Thus, the barrier height between ITO and ZnO is reduced to $\phi'_{Bn} = \phi_{Bn} - \Delta\phi_{pz}$, which results in an increase of thermionic current density through the interface. Likewise, bending of the valance band of ZnO at the electrolyte side could also be reduced due to the remnant positive piezoelectric charges. However, due to the Ohmic-like contact between ZnO and electrolyte, a slight change on the interface band bending contributes a trivial suppression to the effective charge transfer, especially when the original driving force on hole transfer is large. Consequently, a constant ΔJ_{ph} is observed when a tensile strain is maintained in the ZnO PEC anode.

The above analysis clearly shows that ΔJ_{ph} is induced by the piezoelectric polarization, an entirely different mechanism from that of the J_{pz} pulses. ΔJ_{ph} is determined by the interfacial barrier height change due to the remnant polarization, which is a result of the local charge distribution at the interface after the piezopotential-induced charge redistribution reaches equilibrium. This phenomenon is related to the strain and interfacial material properties but is independent of the free charge carriers inside ZnO (at low concentrations). However, J_{pz} is directly related to the apparent piezoelectric potential V_{pz}, and thus the incident light intensity dictates the amplitude of J_{pz}. Under low light intensity, the piezocurrent is more prominent than the constant photocurrent change ($\Delta J_{ph} < J_{pz}$), thus an initial current spike was observed corresponding to J_{pz} (**Figure 8**b and c). Under high light intensity, the piezocurrent merges into a constant photocurrent change ($\Delta J_{ph} > J_{pz}$), thus a square current curve was obtained (Figure 8a).

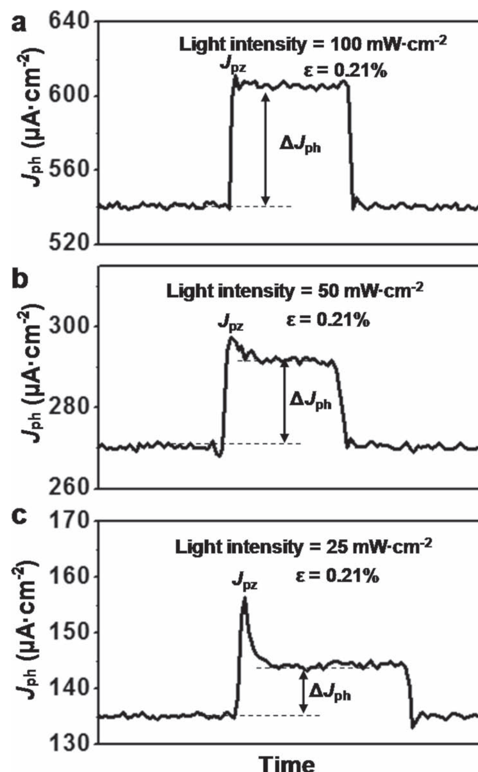

Figure 8. a–c) J_{ph} variation profiles recorded under light intensity of 100, 50, and 25 mW·cm^{-2}, respectively, when the ZnO PEC anode was subjected to a constant 0.21% tensile strain. J_{ph} spikes correspond to the piezopotential-driven charge flow through the external circuit when the piezoelectric polarization is not completely compensated by internal photogenerated charges. They are denoted as J_{pz}. The following constant J_{ph} increase was due to interface barrier height change and is denoted as ΔJ_{ph}.

7. Perspective

In the absence of an external electric field, the polarization density, which is used in piezotronics as the active agent for interface engineering, depends directly upon the linear piezoelectric coefficient and the strain tensor. A more pronounced effect on interface energetics can thus be obtained by utilizing: 1) materials which are capable of sustaining large strains without failure and/or 2) making use of a subclass of piezoelectrics, ferroelectrics, which have pronounced piezoelectric coefficients (>100 pC/N) and attractive semiconductor functionality. The first case results in a more rugged piezoelectric component capable of enduring substantial strain. However, because these materials must themselves either compose the heterointerface of interest or be within the immediate vicinity of said interface, in order to avoid device failure, extreme care must be taken to mediate the additional strain supported by the other materials composing the device. A design where peripheral, robust, strained piezoelectric films sandwich an active semiconductor heterojunction located within a neutral strain axis is a conceivable architecture for enhancing piezotronic performance. A key challenge facing the second case, the integration of high performance ferroelectric materials into heterojunction devices, is the low conductivity these materials often exhibit in conjunction with their pronounced piezoelectric coefficients. In devices whose functionality depends upon the transport of charge carriers, this impediment cannot be overstated. A peripheral approach like the one states previously, where the ferroelectric

© 2012 WILEY-VCH Verlag GmbH & Co. KGaA, Weinheim

film itself does not take part in the active heterojunction, can again be used. Alternatively, GaN and many other III–V Wurtzite materials are the core semiconductor components in solar cells, lasers, LEDs, and PEC cells. These materials also exhibit appreciable piezoelectric effect, and thus make good candidates for applying piezoelectric polarization to regulate their semiconductor functionalities.

8. Conclusion

The remnant piezopotential has been used to improve interfacial properties and enhance performance in heterojunction devices, which is a significant aspect of the piezotronic effect. From calculations to proof-of-principle demonstrations, remnant piezopotentials have been used to create local potential wells for enhanced LED quantum efficiency, improved performance in GaN/InGaN quantum well lasers, leveraged to form electromechanical memory diodes, and used to increase open circuit voltage and photocurrent extraction in polymeric solar cells and PECs, respectively. The good qualitative agreement between the PEC experiments and theory allowed a quantitative evaluation and verification of order-of-magnitude results expected from theory. The use of piezopotential has been shown, through use of an analog ferroelectric's remnant polarization, to modulate reacting kinetics at semiconductor/solution interfaces and thus act as a mechanism for addressing the realm of spatially selective catalytic properties. In general, this effect renders a new pathway for engineering the interfacial band structure without altering the interface structure or chemical composition, which is promising for improving the performance of many electronics, optoelectronics, and photovoltaic devices.

Acknowledgements

We thank the support of National Science Foundation under grant No. DMR-0905914, DARPA under grant No. N66001-11-1-4139, and the UW-Madison graduate school.

Received: November 16, 2011
Published online: May 2, 2012

[1] Z. L. Wang, *Adv. Mater.* **2007**, *19*, 889.
[2] Z. L. Wang, *Nano Today* **2010**, *5*, 540.
[3] Z. L. Wang, *J. Phys. Chem. Lett.* **2010**, *1*, 1388.
[4] Z. L. Wang, *Adv. Funct. Materi* **2008**, *18*, 3553.
[5] Y. Zhang, Y. Liu, Z. L. Wang, *Adv. Mater.* **2011**, *23*, 3004.
[6] S. M. Sze, K. K. Ng, *Physics of Semiconductor Devices*, Wiley-Interscience, New Jersey **2007**.
[7] J. H. He, C. L. Hsin, J. Liu, L. J. Chen, Z. L. Wang, *Adv. Mater.* **2007**, *19*, 781.
[8] Y. Hu, Y. Zhang, Y. Chang, R. L. Snyder, Z. L. Wang, *ACS Nano* **2010**, *4*, 4220.
[9] X. D. Wang, J. Zhou, J. Song, J. Liu, N. Xu, Z. L. Wang, *Nano Lett.* **2006**, *6*, 2768.
[10] J. F. Wager, *Thin Solid Films* **2008**, *516*, 1755.
[11] N. W. Ashcroft, N. D. Mermin, *Solid State Physics*, Saunders College Publishing, New York **1976**.
[12] Q. Yang, X. Guo, W. Wang, Y. Zhang, S. Xu, D. H. Lien, Z. L. Wang, *ACS Nano* **2010**, *4*, 6285.
[13] A. Rockett, *The Materials Science of Semiconductors*, Springer, New York **2008**.
[14] X. D. Wang, J. H. Song, J. Liu, Z. L. Wang, *Science* **2007**, *316*, 102.
[15] Y. F. Hu, Y. L. Chang, P. Fei, R. L. Snyder, Z. L. Wang, *ACS Nano* **2010**, *4*, 1234.
[16] W. Z. Wu, Z. L. Wang, *Nano Lett.* **2011**, *11*, 2779.
[17] Y. Zhang, Y. F. Hu, S. Xiang, Z. L. Wang, *Appl. Phys. Lett.* **2010**, *97*.
[18] J. Zhou, Y. D. Gu, P. Fei, W. J. Mai, Y. F. Gao, R. S. Yang, G. Bao, Z. L. Wang, *Nano Lett.* **2008**, *8*, 3035.
[19] M. E. Lines, A. M. Glass, *Principles and Applications of Ferroelectrics and Related Materials*, Oxford, New York **1977**.
[20] R. R. Mehta, B. d. Silverma, J. T. Jacobs, *J. Appl. Phys.* **1973**, *44*, 3379.
[21] D. Damjanovic, *Rep. Prog. Phys.* **1998**, *61*, 1267.
[22] B. H. Park, B. S. Kang, S. D. Bu, T. W. Noh, J. Lee, W. Jo, *Nature* **1999**, *401*, 682.
[23] D. J. Kim, J. Y. Jo, Y. S. Kim, Y. J. Chang, J. S. Lee, J. G. Yoon, T. K. Song, T. W. Noh, *Phys. Rev. Lett.* **2005**, *95*, 4.
[24] I. P. Batra, P. Wurfel, B. d. Silverma, *Phys. Rev. B* **1973**, *8*, 3257.
[25] M. Y. Zhuravlev, R. F. Sabirianov, S. S. Jaswal, E. Y. Tsymbal, *Phys. Rev. Lett.* **2005**, *94*, 246802.
[26] P. E. Bloomfield, I. Lefkowitz, A. D. Aronoff, *Phys. Rev. B* **1971**, *4*, 974.
[27] J. N. Israelachvili, *Intermolecular and Surface Forces*, Academic Press, Boston **2010**.
[28] N. Sato, *Electrochemistry at Metal and Semiconductor Electrodes*, Elsevier, Tokyo **1998**.
[29] J. Zhou, P. Fei, Y. D. Gu, W. J. Mai, Y. F. Gao, R. Yang, G. Bao, Z. L. Wang, *Nano Lett.* **2008**, *8*, 3973.
[30] Q. Yang, W. H. Wang, S. Xu, Z. L. Wang, *Nano Lett.* **2011**, *11*, 4012.
[31] S. H. Park, S. L. Chuang, *Appl. Phys. Lett.* **1998**, *72*, 3103.
[32] Y. Yang, W. Guo, Y. Zhang, Y. Ding, X. Wang, Z. L. Wang, *Nano Lett.* **2011**, *ASAP*.
[33] N. V. Burbure, P. A. Salvador, G. S. Rohrer, *J. Am. Ceramic Soc.* **2006**, *89*, 2943.
[34] P. M. Jones, D. E. Gallardo, S. Dunn, *Chem. Mater.* **2008**, *20*, 5901.
[35] D. Tiwari, S. Dunn, *J. Mater. Sci.* **2009**, *44*, 5063.
[36] S. V. Kalinin, D. A. Bonnell, T. Alvarez, X. Lei, Z. Hu, J. H. Ferris, Q. Zhang, S. Dunn, *Nano Lett.* **2002**, *2*, 589.
[37] J. Shi, M. B. Starr, H. Xiang, Y. Hara, M. A. Anderson, J. H. Seo, Z. Ma, X. D. Wang, **2011**, *11*, 5587.
[38] C. K. Cheung, R. X. Wang, C. D. Beling, A. B. Djurisic, S. Fung, *J. Phys. Condens. Matter* **2007**, *19*, 086204.

© 2012 WILEY-VCH Verlag GmbH & Co. KGaA, Weinheim